Connexin interaction patterns in keratinocytes revealed morphologically and by FRET analysis

Wei-Li Di[1], Yan Gu[2], John E. A. Common[1], Trond Aasen[1], Edel A. O'Toole[1], David P. Kelsell[1] and Daniel Zicha[2],*

[1]Centre for Cutaneous Research, Institute of Cell and Molecular Science, Barts and the London School of Medicine and Dentistry, Queen Mary, University of London, 4 Newark Street, London E1 2AT, UK
[2]Cancer Research UK London Research Institute, Lincoln's Inn Fields Laboratories, 44 Lincoln's Inn Fields, London WC2A 3PX, UK
*Author for correspondence (e-mail: daniel.zicha@cancer.org.uk)

Summary

Multiple connexins, the major proteins of gap junctions, have overlapping expression in the human epidermis and are postulated to have a key role in keratinocyte differentiation and homeostasis. The functional importance of connexins in the epidermis is emphasised by the association of mutations in four human connexins with various hyperproliferative skin disorders. As immunohistochemistry demonstrated overlapping expression of specific connexins in keratinocytes, we performed colocalisation analyses and applied a modified FRET methodology to assess possible heteromeric interactions between different combinations of four wild-type (wt) and mutant connexins. The data generated indicate that there is evidence for multiple connexin interactions at the plasma membrane between (wt)Cx26, (wt)Cx30 and (wt)Cx31 in keratinocytes and thus, the potential for the formation of a large number of different channel types each with different channel properties. In addition, we demonstrate that the inherent in vitro trafficking defect of the skin disease mutations (D50N)Cx26 and (G11R)Cx30 can be overcome partially by the coexpression of different wild-type connexins but this rescue does not result in large gap junction aggregates at the plasma membrane. These data indicate that skin disease associated Cx26 or Cx30 mutations are likely to disrupt a number of different channel types important in distinct aspects of keratinocyte biology.

Key words: Connexin, FRET, Keratinocyte, Skin disease

Introduction

The ability of cells to communicate with each other via gap junctions is important in the maintenance of normal tissue homeostasis. Gap junctions are clusters of double-membrane channels formed by two hemi-channel transmembrane protein structures termed connexons. Each connexon is made up of six transmembrane protein subunits named connexins. Connexons are formed in the endoplasmic reticulum (ER) and then delivered in vesicular carriers to the plasma membrane. Though it should be noted that there are multiple intracellular trafficking pathways involved with the transport of different connexins to the plasma membrane (Martin et al., 2001). Once at the plasma membrane, they cluster into hemichannel plaques and move laterally along the plasma membrane into the gap between two cells (Lal and Lin, 2001; Lauf et al., 2002; Yeager et al., 1998). The docking of two connexons at cell-cell appositions results in the formation of a gap junction channel that facilitates the diffusion of ions and low molecular weight metabolites or signalling molecules between cells. Thus, gap junctions provide a mechanism of synchronised cellular response facilitating the metabolic and electrical functions of cells by the direct intercellular transfer of ions and small molecules (Kelsell et al., 2001b). Open connexons found at the non-junctional plasma membrane (termed hemichannels) connect the cell interior with the extracellular environment and appear to play a role in paracrine signalling (Goodenough and Paul, 2003). There are 20 identified human connexin genes (Willecke et al., 2002) and, in many tissues, multiple connexins are co-expressed. For example, at least ten human connexins are expressed in the human epidermis in overlapping, but also distinct, keratinocyte sub-populations (Di et al., 2001b). This complex pattern of connexin expression in many tissue types suggests that there may be distinct cellular roles for individual or subgroups of connexins. Indeed intercellular channels have distinct permeabilities and selectivities for different molecules such as ATP, AMP and IP3 depending on their connexin composition (Bevans et al., 1998; Goldberg et al., 1999; Goldberg et al., 2002; Saez et al., 2003). Further levels of complexity arise owing to the ability of specific connexins to interact heteromerically and heterotypically, for example, Cx43 and Cx40 (He et al., 1999; Kumar and Gilula, 1996). Thus there is a potential for a myriad of distinct intercellular channel types within any cell and tissue.

Compelling evidence for diverse physiological roles for connexins have come from the association of connexin mutations with human disease and from genetically manipulated mice. Germline mutations in connexin genes have been demonstrated in a variety of human diseases including demyelinating neuropathy, hearing loss, epidermal disorders and lens cataracts (Kelsell et al., 2001a). Gene-targeting studies in mice have also revealed additional phenotypes including female sterility and defective cardiac conduction (White and

Paul, 1999). Cx26 mutations are associated with non-syndromic autosomal recessive sensorineural hearing loss (Kelsell et al., 1997) and account for a significant proportion of genetic hearing loss (Denoyelle et al., 1997; Meyer et al., 2002; Zelante et al., 1997). Although a classical mouse knockout of Cx26 was lethal in utero, the hearing loss phenotype observed in human Cx26 'knockouts' has been replicated from gene targeting studies using an inner ear-specific gene promoter in the mouse (Cohen-Salmon et al., 2002; Kudo et al., 2003; Teubner et al., 2003). Like the sensory epithelium in the inner ear, there are abundant gap junctions in the epidermis. Distinct dominant Cx26 mutations have also been shown to cause not only non-syndromic hearing loss but also syndromes affecting other ectodermal-derived tissues. In these syndromes, abnormal epidermal keratinization is the common feature (Kelsell et al., 2001a; Richard, 2003). The additional identification of skin disease associated mutations in three other connexins Cx31, Cx30 and Cx30.3 demonstrate that intercellular communication via gap junctions is an important mechanism by which the normal epidermis differentiates (Richard, 2003). These genetic studies also suggest that different mutations in the same connexin have distinct effects on epidermal differentiation and the sensory epithelia of the inner ear. The further investigation of these genotype-phenotype differences at the molecular and cellular level are providing valuable insights into the role of connexins in intercellular communication via gap junctions and possibly other aspects of cell biology.

As there is co-localisation of connexins in many keratinocytes and within inner ear cell subpopulations and as connexins can form heteromeric connexons, it would be reasonable to suggest that dominant disease-associated mutations in a specific connexin may affect the assembly and functionality of other connexins. In this study, we have performed colocalisation analyses and applied a modified Fluorescence Resonance Energy Transfer (FRET) methodology to investigate direct connexin interactions between different wild-type and skin disease associated mutant connexins in keratinocytes.

Materials and Methods

Construction of chimeric wild-type and mutant Cx-EGFP/ECFP/EYFP

The full-length coding region of human wild-type (wt) connexin Cx26 or Cx30 or Cx31 or Cx30.3 were amplified by PCR using gene-specific primers with added *Hin*dIII restriction site sequences on the forward primer and *Sal*I sequence on the reverse primer to aid cloning. The PCR products were inserted into the pEGFP-N1 or pECFP-N1 or pEYFP-N1 vector (Clontech, Hampshire, UK). The EGFP or ECFP or EYFP was fused at the C-terminus of the connexin protein and the stop codon altered to allow expression of the fluorescent connexin fusion proteins. The two skin disease associated connexin mutations D50N and G11R were introduced into (wt)Cx26- and (wt)Cx30-EGFP/ECFP/EYFP, respectively, by site-directed mutagenesis (SDM) using the QuickChange SDM kit (Stratagene, La Jolla, CA, USA) according to the manufacturer's instructions. All positive clones were identified by restriction enzyme analysis and DNA was sequenced to check that no erroneous sequence changes had occurred. The sequences of the oligonucleotide primers used are listed in Table 1.

Tissue and cell culture

Skin biopsies were obtained after ethical approval and patient consent from an individual with autosomal dominant Keratitis-Ichthyosis-Deafness (KID) syndrome who is heterozygous for the D50N mutation in *GJB2* encoding Cx26 (Common et al., 2003) and an individual with autosomal dominant Hidrotic Ectodermal Dysplasia (HED) who is heterozygous for the G11R mutation in *GJB6* encoding Cx30 (Common et al., 2002). Frozen sections from these biopsies were analysed by immunohistochemistry. The immortalized keratinocytes NEB1 (Morley et al., 1995) were maintained in 3:1 DME:Ham F12 medium supplemented with 10% FCS and other supplements as described previously (Di et al., 2002). We have previously shown that NEB1 cells express low levels of a number of connexins including Cx26 and 30, with higher levels of Cx31 within a subpopulation of the NEB1 keratinocytes (Di et al., 2002).

Transfection

1×10^5 NEB1 cells were plated on 13 mm glass coverslips 24 hours before transfection. The NEB1 cells were transfected with 1 µg plasmid DNA using Transfast reagent (Promega, Southampton, Hants, UK) according to the manufacturer's protocol. Co-transfections with two constructs were done at a 1:1 ratio. 24 hours post transfection, cells were fixed with 4% buffered paraformaldehyde for 20-30 minutes and mounted on slides with solution containing 10% Mowiol D488 (Calbiochem, Nottingham, UK), 25% glycerol and 2.5% 1.4-diazabicyclo[2.2.2]octane (Sigma, Poole, Dorset, UK) in 50 mM Tris-HCl, pH 8.5. Slides were kept at –20°C until assayed for FRET.

Immunofluorescence

Immunofluorescence staining was performed in tissue as described previously (Di et al., 2002). Purified rabbit polyclonal Cx26 antibody (Di et al., 2001a), rabbit polyclonal Cx30 antibody (Zymed, Cambridge Bioscience, UK) or monoclonal β-actin antibody (Sigma, Poole, Dorset, UK) was used as primary antibody. As no commercial Cx30.3 was available, a polyclonal antibody was raised to a unique peptide sequence corresponding to amino acids 248-266 in the cytoplasmic region of human Cx30.3. Alexa 488 goat anti-rabbit IgG antibody or Alexa 546 rabbit anti-mouse IgG antibodies (Molecular Probes, Oregon, USA) were used for secondary antibodies. After staining, slides were mounted in Mowiol solution and kept at 4°C prior to confocal microscopy. Fluorescence images were recorded using a LSM 510 META laser-scanning confocal microscope (Carl Zeiss) and processed using Adobe Photoshop 6.0. Fluorescence images of NEB1 cells transfected with ECFP and EYFP fusion constructs were also taken with the LSM 510 META. The images are presented using cyan and yellow pseudocolour look-up tables, which were designed to produce white in the merged images when perfectly colocalised.

Fluorescence resonance energy transfer (FRET) assay

Experimentally, FRET can be detected by various techniques (Eidne et al., 2002; Lippincott-Schwartz et al., 2001; Wouters et al., 1998). One of the frequently used approaches is the acceptor depletion FRET (adFRET), which retrieves the steady state FRET information by measuring the donor fluorescence variation before and after acceptor photobleaching (Sekar and Periasamy, 2003; Wouters et al., 1998). One of the difficulties of implementing adFRET is separating the spectral bleed-through (SBT), that is, the acceptor emission contribution to the donor channel, and the donor photobleached by the acceptor photobleaching laser. For example, with a standard donor-acceptor pair ECFP-EYFP and 458 nm laser excitation, SBT can be 23.8% from ECFP into the acceptor channel and 12.0% from EYFP into the donor channel. In this study, we have applied a specially developed quantitative adFRET approach combining linear spectral unmixing with adFRET (u-adFRET) to solve the SBT problem (Gu et al., 2004). As the SBT is addressed in advance, the donor enhancement revealed by the acceptor photobleaching is solely from the FRET (Fig. 1). Fixed cells co-transfected with Cx-ECFP (donor) and Cx-EYFP (acceptor)

Table 1. Primer sequences

Name	Genotype	Phenotype	Primers (5′–3′)
(wt)Cx26–ECFP/EYFP*	Wild type	–	Forward: GCGAAGCTTATGGATTGGGGCACGCTGCA Reverse: GCGGTCGACCATCCAACTGGCTTTTTTG
(wt)Cx30–ECFP/EYFP*	Wild type	–	Forward: GCGAAGCTTATGGATTGGGGGACGCTGC Reverse: GCGGTCGACCATCCGCTTGGGAAACCTG
(wt)Cx31–ECFP/EYFP*	Wild type	–	Forward: GCGAAGCTTATGGACTGGAAGACACTC Reverse: GCGGTCGACCATCCGATGGGGGTCAGGT
(wt)Cx30.3–ECFP/EYFP*	Wild type	–	Forward: GCGAAGCTTATGAACTGGGCATTTCTGCA Reverse: CGGTCGACCATCCTGGATACCCACCTGC
(D50N)Cx26–ECFP/EYFP†	D50N	KID	GGAGATGAGCAGGCC**AA**CTTTGTCTGCAACACCCTGC
(G11R)Cx30–ECFP/EYFP†	G11R	HED	CGCTGCACACTTTCATC**A**GGGGTGTCAAC

*Restriction enzyme sites underlined.
†The mutated site is bold and mutated codon underlined.

were examined with a Zeiss LSM 510 META confocal microscope (63× NA 1.4 oil-immersion objective). Four to five fields with fluorescent cells were selected on each slide and up to five regions of interest (ROIs) within each cell were photobleached. Images were acquired from eight spectral channels simultaneously, covering important parts of the emission from both fluorophores (474-549 nm) with 11 nm spectral resolution. Two argon laser lines were used. The 458 nm laser line was used for imaging as it can excite both ECFP and EYFP. The 514 nm laser line was used for the acceptor photobleaching because it only excites EYFP. The imaging laser was adjusted so that photobleaching throughout the acquisition was negligible. The acceptor photobleaching required full laser power (0.1 mW), and was repeated 100 times over pre-selected ROIs to make sure that the overall acceptor population within each ROI was eliminated. The imaging procedure commenced with pre-photobleaching acquisition until a preset time point, after which the imaging laser was turned off and the acceptor photobleaching started. The imaging laser was turned on again after photobleaching for the post-photobleaching acquisition. The changes of fluorescence intensity from acquired image sequence were processed using the u-adFRET algorithm implemented in Mathematica© (Wolfram Research). Two controls labelled with either ECFP or EYFP only were imaged in advance in order to establish the reference spectra for the spectral unmixing during the FRET measurements.

Immunoprecipitation

Cells were transfected with Cx-EGFP plasmid(s) using Fugene (Roche) according to the manufacturer's protocol in 100 mm dishes. Cells were washed in PBS twice and lysed (48 hours post transfection) in 0.5 ml ice-cold immunoprecipitation buffer containing 1% Triton X-100, 150 mM NaCl, 10 mM Tris-HCl (pH 7.4), 1 mM EDTA (pH 8.0), 1 mM EGTA, 0.5% NP-40, 1 mM sodium orthovanadate and complete protease inhibitor cocktail (Roche). All steps were performed on ice. After a 30-minute incubation, cells were scraped into 1.5 ml Eppendorf tubes and centrifuged at 12,000 **g** for 10 minutes and the supernatant was transferred to a new tube. The lysate was pre-cleared using 80 µl Protein G-sepharose
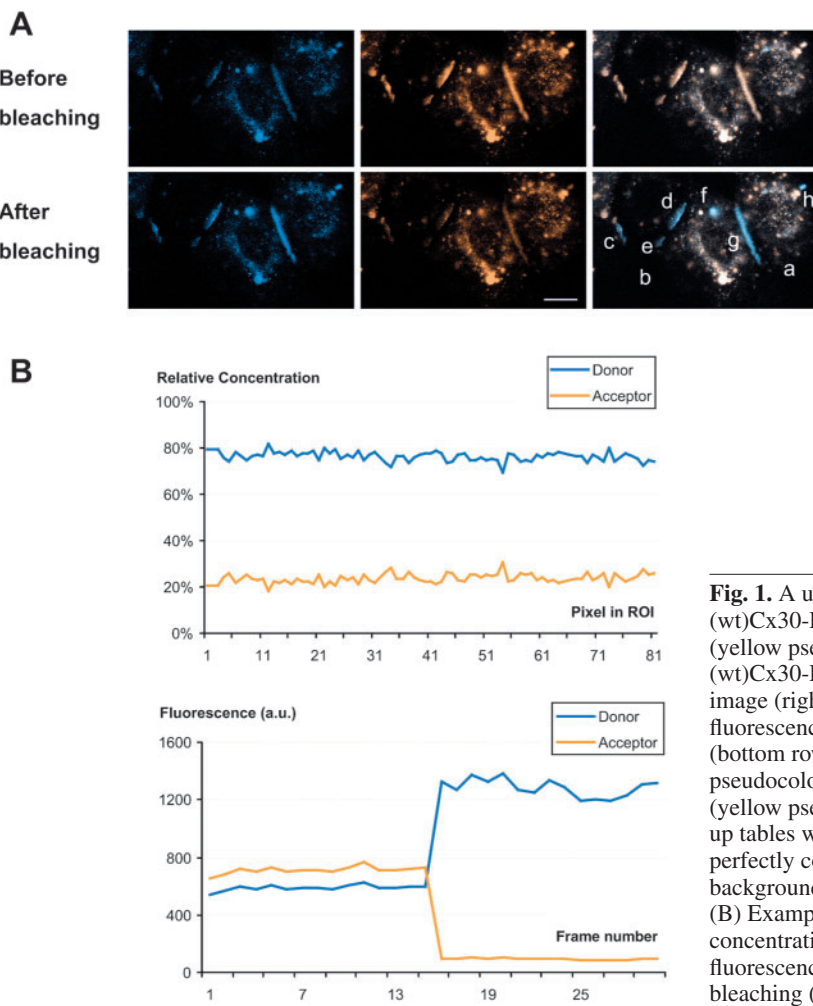

Fig. 1. A u-adFRET assay. Keratinocytes were co-transfected with (wt)Cx30-ECFP (cyan pseudocolour, donor) and (wt)Cx26-EYFP (yellow pseudocolour, acceptor). (A) Expression patterns of (wt)Cx30-ECFP (left), (wt)Cx26-EYFP (middle) and the merged image (right) before bleaching (top row) and the changes of fluorescence intensity in areas of interest (c to h) after bleaching (bottom row) show enhanced fluorescence intensity of donor (cyan pseudocolour, left) and reduced fluorescence intensity of acceptor (yellow pseudocolour, middle). Cyan and yellow pseudocolour look-up tables were designed to produce white in the merged image when perfectly colocalised. Areas labelled a and b were used as a background reference and an unbleached reference respectively. (B) Example profiles (from region g) of relative expression concentrations of donor and acceptor (top) and the changes of fluorescence intensity in donor and acceptor before and after bleaching (bottom). Bar, 10 µm.

beads (50% slurry, Amersham) mixing for 1 hour at 4°C followed by a 1-minute centrifugation at 12,000 *g* to remove the beads. 4 µg antibody was added and incubated overnight at 4°C with gentle shaking. To precipitate any complex, 80 µl Protein G-sepharose suspension was added and mixed for 2 hours. The pellet was collected by centrifuging for 30 seconds at 12,000 *g* and washed four times with 1 ml immunoprecipitation buffer, centrifuging between each wash as before. The final pellet was suspended in 100 µl sample buffer [125 mM Tris-HCl, pH 6.8, 4% SDS, 20% glycerol, 2% DTT, 1 mM sodium orthovanadate, protease inhibitor cocktail (Roche) and 0.006% Bromophenol Blue], boiled at 95°C for 5 minutes followed by brief vortexing and centrifugation to remove the beads.

Samples were loaded on standard 12% SDS-PAGE gels. Membranes were incubated in PBS-0.1% Tween-20 containing 5% dry milk powder for 1 hour. An anti-GFP-HRP antibody (130-091-833, Miltenyi Biotech, Surrey, UK) was used (1:10,000 in blocking buffer for 1 hour) in order to avoid non-specific IgG bands (from using secondary HRP antibodies), followed by standard ECL analysis (Amersham).

Results

In vivo localisation of different wild-type and mutant connexins

Antibodies against human Cx26, Cx30, Cx31 and Cx30.3 were used on normal interfollicular human skin to demonstrate the pattern of localisation of these connexins in normal skin (Fig. 2). The Cx30.3 antibody clearly demonstrates that Cx30.3 protein has a punctate localisation at the plasma membrane in keratinocytes within the stratum granulosum of the epidermis. As described previously (Di et al., 2001b), Cx31 is also specifically expressed in this epidermal layer whereas Cx30 is also expressed in keratinocytes within the spinous spinosum. In normal interfollicular epidermis, Cx26 protein is not detected and has been detected previously only in hyperproliferative skin such as the palmoplantar or diseased/damaged epidermis (Di et al., 2001b; Lucke et al., 1999). However, Cx26 protein is easily detectable in the sweat glands of normal epidermis.

Cx26 and Cx30 antibodies were also used on biopsies of lesional interfollicular skin obtained from HED patient heterozygous for the G11R mutation in *GJB6* encoding Cx30 and also from the KID syndrome patient heterozygous for the D50N mutation in *GJB2* encoding Cx26. The localisation data was compared to that seen in normal skin. A punctate staining pattern of Cx30 was observed in the stratum granulosum of the epidermis with some evidence for the presence of positive staining at the plasma membrane. Plasma membrane localisation of Cx26 can clearly be observed in the sweat glands from the KID patient heterozygous for the (D50N)Cx26 mutation. A similar in vivo localisation was described for Cx26 in a skin biopsy taken from a KID patient who had inherited the S17F mutation in *GJB2* (Richard et al., 2002). These in vivo data are in contrast with previous in vitro observations in which skin disease associated mutant connexins had primarily a cytoplasmic localisation and a plasma membrane trafficking defect (Common et al., 2002; Common et al., 2003; Di et al., 2001a). For example, (D50N)Cx26-EGFP or (G11R)Cx30-EGFP proteins displayed a perinuclear compartmental staining pattern in transfected keratinocytes. These differences between in vivo and in vitro studies suggest that connexin-connexin interactions in vivo may change mutant protein behaviour with respect to morphology, localisation and, possibly, functionality. This hypothesis was investigated with the following experiments.

Colocalisation of wild-type connexins in vitro

Before investigating the effect of the two mutant connexins on wild-type connexins, coexpression and localisation studies of different pairs of four wild-type connexins were performed to assess homomeric interactions and to determine if heteromeric wild-type connexin interactions occur. The C-termini of (wt)Cx26, (wt)Cx30, (wt)Cx31 and (wt)Cx30.3 were tagged with the fluorescent reporter ECFP or EYFP. These (wt)Cx-
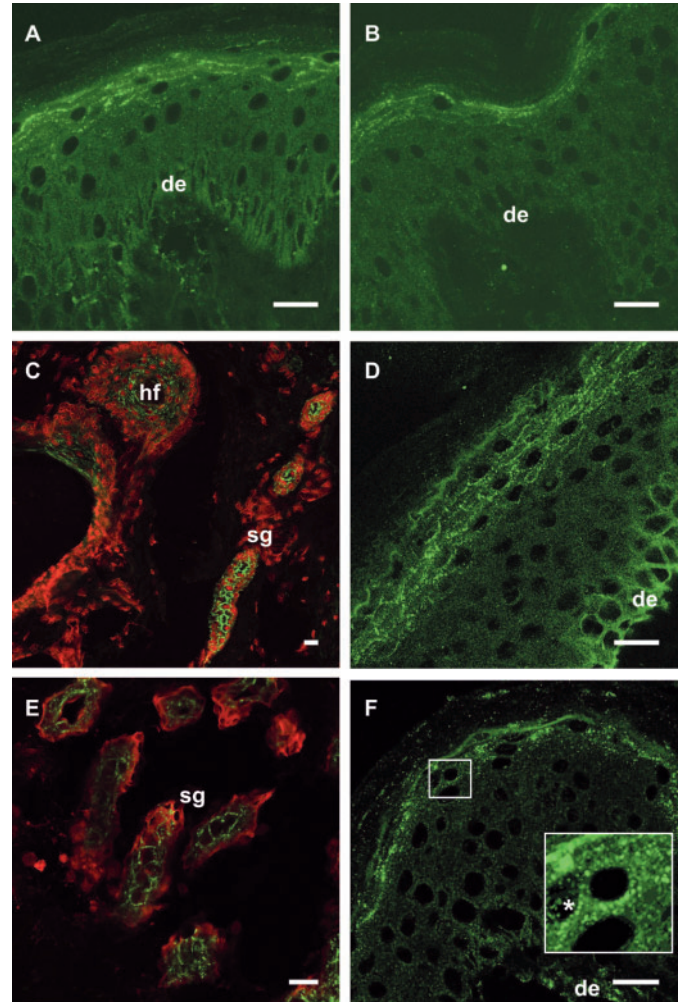

Fig. 2. Immunofluorescence staining of connexins in skin. Green fluorescence represents anti-connexin antibody (A to F) and red fluorescence (C and E) represents anti-β-actin antibody. (A) Cx30.3 and (B) Cx31 both localised in the stratum granulosum of control epidermis. (C) Cx26 expression in the hair follicle (hf) and sweat gland (sg) of control skin (note that Cx26 is undetectable in normal interfollicular epidermis). (D) Cx30 expression was clearly localised at the plasma membrane of keratinocytes in the upper epidermal layers of control epidermis. (E) Cx26 expression in the sweat glands (sg) of skin from the KID patient heterozygous for the D50N mutation in Cx26 was comparable to that seen in control skin. (F) Interfollicular skin obtained from the HED patient heterozygous for the G11R mutation in Cx30 was stained by Cx30 antibody and revealed a sparse staining pattern with some protein detectable at the plasma membrane. An enlargement of the small, boxed area is shown. Asterisk indicates probable localisation of aggregated Cx30 protein at the plasma membrane in keratinocytes of the stratum granulosum. de, position of dermal-epidermal junction. Bar, 20 µm.

Fig. 3. FRET images of homomeric connexin formation in NEB1 keratinocytes. The first three rows show pairs of cells co-transfected with (wt)Cx26-ECFP and (wt)Cx26-EYFP, (wt)Cx30-ECFP and (wt)Cx30-EYFP, and (wt)Cx31-ECFP and (wt)Cx31-EYFP. These co-transfections clearly show large gap junction-like aggregates of the fusion proteins at the cell-cell interface. In contrast the three cells in contact presented in the fourth row co-transfected with (wt)Cx30.3-ECFP and (wt)Cx30.3-EYFP did not show any aggregates at the plasma membrane. Left-hand panels are (wt)Cx-ECFP images, middle panels, (wt)Cx-EYFP images and right-hand panels, merged images. Bar, 10 μm.
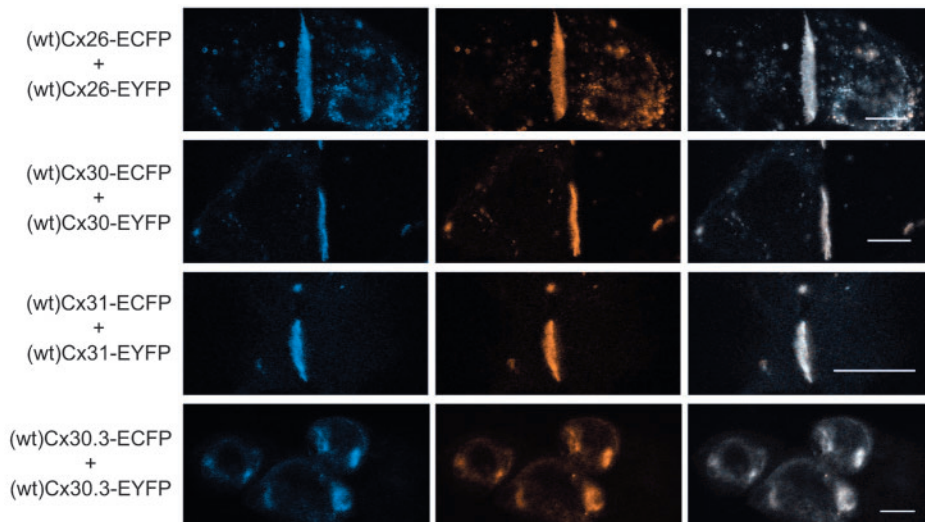
ECFP/EYFP fusion proteins were expressed in the NEB1 keratinocytes after co-transfection. (wt)Cx26-ECFP/EYFP, (wt)Cx30-ECFP/EYFP and (wt)Cx31-ECFP/EYFP assembled into typical gap junction-like aggregates as fluorescent puncta and lines in the adjoining plasma membranes of cells (Fig. 3). In contrast, (wt)Cx30.3-ECFP/EYFP revealed a large bright fluorescence mass in the cytoplasm, specifically displaying a perinuclear localisation, without any gap junction-like aggregates at the plasma membrane. A similar localisation was observed with transfected untagged (wt)Cx30.3 constructs following cell fixation and immunostaining with the Cx30.3 antibody (data not shown). However, in vivo data clearly shows that endogenous (wt)Cx30.3 is able to traffic to the plasma membrane in differentiated keratinocytes (Fig. 2). Co-transfections were also carried out with two different (wt)Cx-ECFP/EYFP constructs. Images showed that there were

colocalised gap junction-like aggregates of (wt)Cx26+(wt)Cx30, (wt)Cx30+(wt)Cx31, and (wt)Cx26+(wt)Cx31 (Fig. 4). However, although there was colocalisation of (wt)Cx30.3 with either (wt)Cx31 or (wt)Cx30 or (wt)Cx26, no gap junction-like aggregates formed indicating that (wt)Cx30.3 was inhibiting the trafficking of the other wild-type connexins. No obvious cell phenotypes were observed with the expression of (wt)Cx30.3 alone or when co-transfected with other wild-type connexins.

Colocalisation of wild-type and mutant connexins in vitro

NEB1 cells were co-transfected with ECFP- or EYFP-tagged (wt)Cx26 or (wt)Cx30 or (wt)Cx31 plus mutant (D50N)Cx26 constructs. Imaging showed that (D50N)Cx26-ECFP and (D50N)Cx26-EYFP had a perinuclear localisation (Fig. 5) as seen before with other skin disease associated Cx26 (or Cx30) mutant proteins expressed in vitro (Common et al., 2002; Di et al., 2001a). But there was a change in intracellular localisation when the (D50N)Cx26 tagged construct was co-transfected with (wt)Cx26, (wt)Cx30 and (wt)Cx3 (Fig. 5). Punctate fluorescence at the plasma membrane was seen in 20-30% of the co-transfected cells. Co-transfections were also performed for ECFP/EYFP tagged (wt)Cx26 or (wt)Cx30 or (wt)Cx31 with mutant (G11R)Cx30 (Fig. 6). The images showed that upon coexpression, a punctate localisation was observed with all three wild-
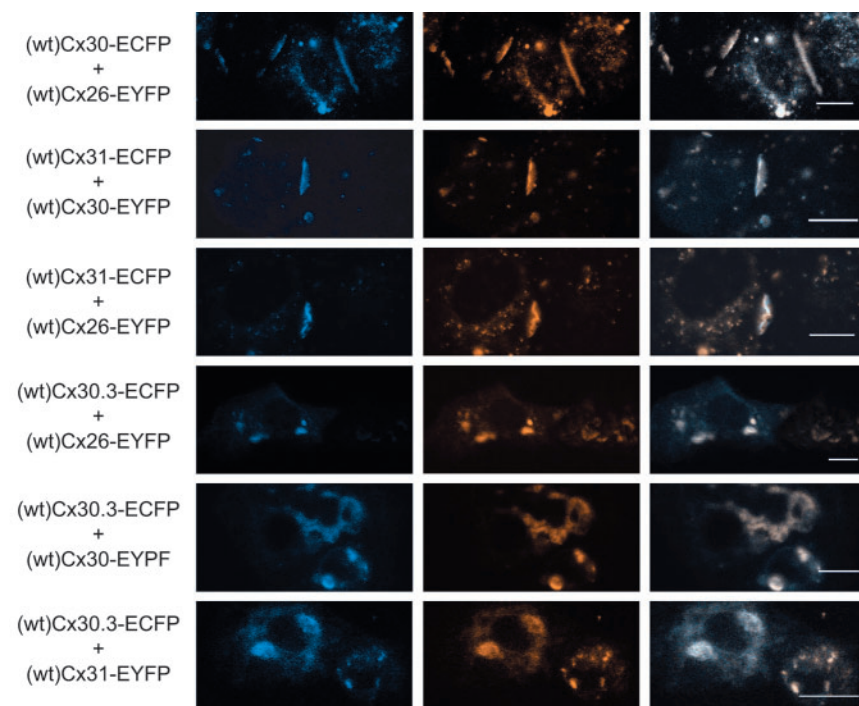

Fig. 4. Images of heteromeric connexin formations in NEB1 keratinocytes. Cells were co-transfected with different pairs of wild-type connexins (Cx) fused with ECFP or EYFP. Left-hand panels, Cx-ECFP images, middle panels, Cx-EYFP images and right-hand panels, merged images. Co-transfection with different combinations of (wt)Cx26, (wt)Cx30 and (wt)Cx31 clearly show large gap junction-like aggregates of the fusion proteins at the cell-cell interface. In contrast, none of the combinations with (wt)Cx30.3 showed any aggregates at the plasma membrane. Bar, 10 μm.
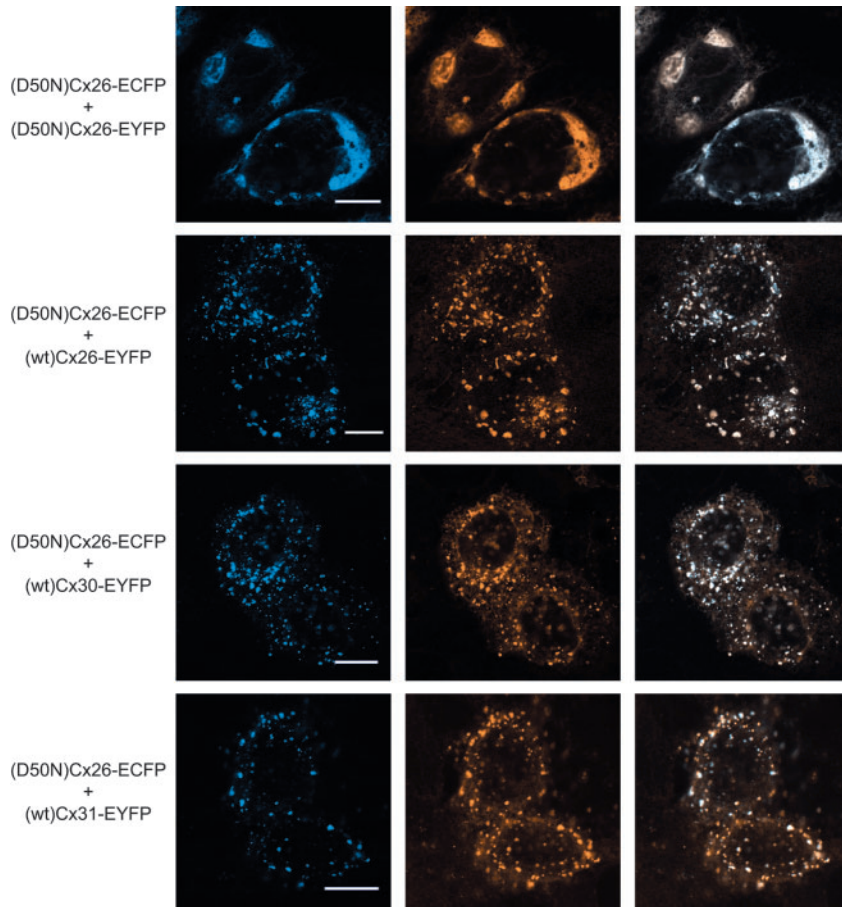
Fig. 5. Images of localisation patterns of mutant (D50N)Cx26 and wild-type connexins in co-transfected NEB1 keratinocytes. Cells were co-transfected with a combination of two constructs at a ratio of 1:1. Unlike (D50N)Cx26 on its own, any combination of (D50N)Cx26 with wild-type connexin produced a punctate pattern of localisation in the cytoplasm. Left-hand panels are Cx-ECFP images, middle panels Cx-EYFP images and right-hand panels merged images of Cx-ECFP and Cx-EYFP. Bar, 10 μm.

conducted separately, the results from the two possible combinations of ECYP- and EYFP-tagged constructs were pooled together after the significance of the pair was tested (ANOVA, $P>0.05$). For quantitative measurement, mean values from ROIs, including FRET efficiency, concentration ratios and acceptor emissions, were used as estimates within corresponding regions. The evaluation was confined to samples that had relative concentrations (donor/acceptor) between 0.33 and 3.00 in order to avoid calculation errors caused by low signal-to-noise ratio, and FRET efficiency saturation owing to high concentrations of donor/acceptor. Table 2 presents mean FRET efficiency values of different wild-type connexin combinations. The standard deviations of FRET efficiency describe the concentration-related distributions within the test regions, rather than errors of measurements. Interestingly, the FRET efficiency of various combinations of wild-type connexins demonstrated different degrees of selectivities. Although (wt)Cx26+(wt)Cx30 has a FRET efficiency value of 32.1±15.0%, which is between that of homomeric (wt)Cx26 (24.7±13.0%) and (wt)Cx30 (36.8±13.0%), FRET efficiency of both (wt)Cx26+(wt)Cx31 (15.0±11%) and (wt)Cx30+(wt)Cx31 (22.6±15%) was lower than that of homomeric (wt)Cx31 (36.0±11%). Though the combination of (wt)Cx30.3 with another connexin significantly improved FRET efficiency (Table 2), (wt)Cx30.3 was still unable to aggregate on the plasma membrane. These phenomena are clearly indicated by the distributions of FRET efficiency via relative concentrations and acceptor emissions (Fig. 7). The FRET efficiency for homomeric mutant connexons was not measured. In support of the FRET interaction data, coexpression of two different wild-type connexin pairs followed by immunoprecipitation demonstrated that physical complexes of (wt)Cx26 and (wt)Cx30 plus (wt)Cx26 and (wt)Cx30.3 could be formed (Fig. 8).

It has been reported that (wt)Cx26 can 'rescue' its mutant (D50N)Cx26 in terms of enabling the mutant protein to traffick to the plasma membrane (Marziano et al., 2003). This observation is confirmed to some degree from our colocalisation (Fig. 5) and FRET experiments. We have observed aggregation of connexons at the plasma membrane in 12 of 27 test cells (44%). A similar phenomenon was found with (wt)Cx31+(D50N)Cx26 in 17 of 44 test cells (39%). In contrast to (D50N)Cx26, the selectivity of (G11R)Cx30 in association with wild-type connexins seems less obvious. Gap junction-like aggregates were detected in combinations of (G11R)Cx30+(wt)Cx26 (3% of test ROIs), (G11R)Cx30+(wt)Cx30 (11%), and (G11R)Cx30+(wt)Cx31 (4%). Mean FRET efficiency shown in Table 2 also confirms that (G11R)Cx30+(wt)Cx30 has the strongest interaction or most compact proximity, whereas (G11R)Cx30+(wt)Cx31 has a weaker interaction. Interestingly, G11R mutation of Cx30 does not affect its interaction with

type connexins. In addition, when coexpressed with wild-type connexin constructs in particular (wt)Cx30 and (wt)Cx26, (G11R)Cx30 could also traffick to the plasma membrane to form gap junction-like aggregates. However, the number of cells with such aggregates was low and the aggregate sizes were small compared to those seen in cells transfected with wild-type connexins alone.

FRET defined interactions between connexins in vitro

Using the u-adFRET approach, FRET efficiency was measured within cells co-transfected with different combinations of connexin constructs tagged with either ECFP or EYFP. The number of cells measured for each combination is shown in Table 2. Several ROIs were chosen from different areas within each cell, such as at gap junction-like aggregates, the plasma membrane or within the cytoplasm, where mean values were extracted. FRET measurements showed that the exchange of fluorophore tags from one construct to another for example, (wt)Cx26-ECFP+(wt)Cx30-EYFP to (wt)Cx26-EYFP+(wt)Cx30-ECFP, did not significantly influence FRET efficiency. Therefore, although the measurements were

(wt)Cx31 as the two combinations have a similar mean FRET efficiency.

Discussion

Previously, EGFP tagged wild-type or mutant connexin fusion proteins have been used to study details of mutant connexins with regard to junction assembly and function in keratinocytes, fibroblasts and HeLa cells. Following transfection or microinjection of these constructs into these cell lines, wild-type connexin proteins are able to traffick to the membrane and form functional gap junction plaques indicated by dye transfer (Common et al., 2002; Di et al., 2002; Marziano et al., 2003). However, the skin disease associated mutant proteins display limited trafficking with a primarily cytoplasmic localisation. In contrast, hearing loss associated mutations are capable of forming large gap junction-like plaque structures at the plasma membrane but unable to transfer dye. These data suggest that there are clear in vitro differences in the cellular processing of the connexin dependant upon whether the mutation causes skin disease or deafness and also in the cell type where it is expressed.

In this study, in vivo analyses of skin biopsies from patients harbouring dominant skin disease associated Cx26 or Cx30 mutations revealed endogenous protein localisation differences to that data generated from transfection studies of constructs expressing mutant connexins. Specifically, in vivo data indicate that connexin protein can be detected at the plasma membrane whereas in vitro data indicate a striking trafficking defect associated with the mutant protein in transfected cells. These in vivo data suggest that the presence of mutant protein at the plasma membrane may be due to the effect of interaction with other wild-type connexins. In order to address these possible interactions, co-transfections and FRET analyses were performed with different combinations of wild-type and mutant human connexins.

Direct observation of transfected cells indicated that (wt)Cx26, (wt)Cx30 and (wt)Cx31 form homotypic gap junction-like structures, whereas (wt)Cx30.3 protein was not detected at the plasma membrane. In addition, cells co-transfected with different pairings of (wt)Cx26, (wt)Cx30 and (wt)Cx31 constructs were also able to form gap junction-like aggregates but to varying degrees. These data indicate that multiple connexon combinations are possible in vivo. (wt)Cx30.3 was unable to traffic to the plasma membrane even upon coexpression and interaction with (wt)Cx31, (wt)Cx30 or (wt)Cx26. The localisation data differ to the in vivo data presented in this study and that of a recent in vitro study suggesting that (wt)Cx31 could relocate (wt)Cx30.3 to the plasma membrane and form gap junction-like aggregates (Plantard et al., 2003). A possible answer to these two different observations could be related to the constructs used and/or the specific cell type in which the transfection was performed. With
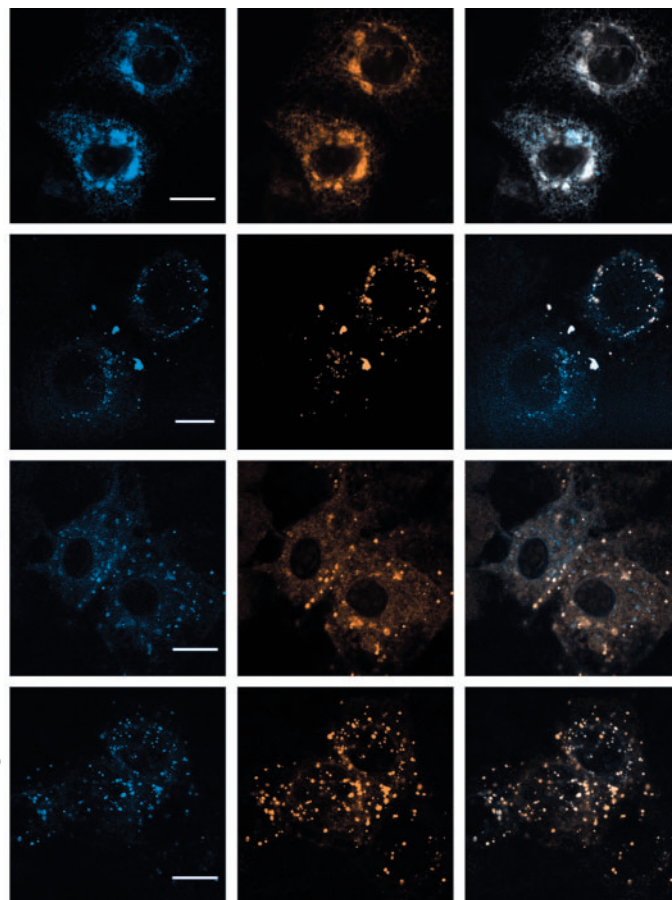

Fig. 6. Images of localisation patterns of mutant (G11R)Cx30 and wild-type connexins in co-transfected NEB1 keratinocytes. Cells were co-transfected with a combination of two constructs at a ratio of 1:1. Unlike (G11R)Cx30 on its own, any combination of (G11R)Cx30 with wild-type connexin produced a punctate pattern of localisation in the cytoplasm. Additionally combinations of (G11R)Cx30 with (wt)Cx26 or (wt)Cx30 produced small aggregates at cell-cell contacts. Left-hand panels are Cx-ECFP images, middle panels, Cx-EYFP images and right-hand panels, merged images of Cx-ECFP and Cx-EYFP. Bar, 10 μm.

Table 2. FRET efficiencies calculated for donor/acceptor concentration ratio between 0.33 and 3.00

| Connexin combination	Number of cells	Number of ROIs	FRET efficiency mean±s.d. (%)
(wt)Cx30 + (wt)Cx30	33	59	37±13
(wt)Cx31 + (wt)Cx31	26	51	36±11
(wt)Cx26 + (wt)Cx30	51	102	32±15
(wt)Cx26 + (wt)Cx26	35	66	24±13
(wt)Cx30 + (wt)Cx31	63	94	23±15
(wt)Cx31 + (wt)Cx30.3	37	92	21±14
(wt)Cx26 + (wt)Cx30.3	38	108	19±15
(wt)Cx26 + (wt)Cx31	65	117	15±11
(wt)Cx30 + (wt)Cx30.3	26	74	14±10
(wt)Cx30.3 + (wt)Cx30.3	16	47	9±7
(wt)Cx30 + (G11R)Cx30	42	142	29±13
(wt)Cx26 + (G11R)Cx30	44	187	26±14
(wt)Cx26 + (D50N)Cx26	27	135	24±12
(wt)Cx31 + (G11R)Cx30	37	137	22±12
(wt)Cx31 + (D50N)Cx26	44	260	21±14
(wt)Cx30 + (D50N)Cx26	28	129	20±13
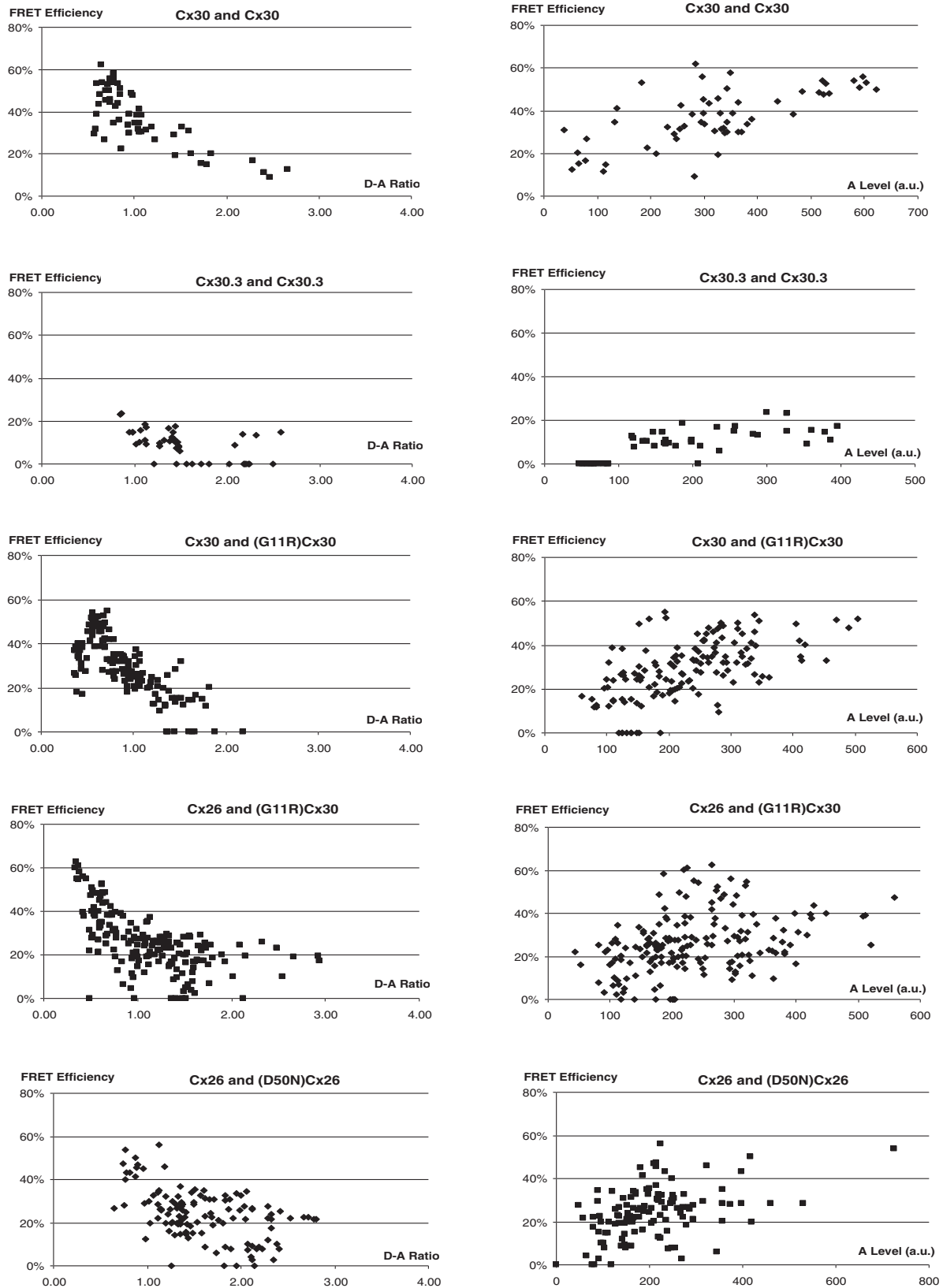
Fig. 7. Mean FRET efficiency as a function of relative concentration ratio of donor/acceptor (Cx-ECFP/Cx-EYFP) and acceptor fluorescence intensity level for different combinations of connexins. The decrease of FRET efficiency with the increase of donor/acceptor concentration ratio, but its insensitivity to the increase of absolute acceptor level, indicate that donors and acceptors are clustered into connexons.
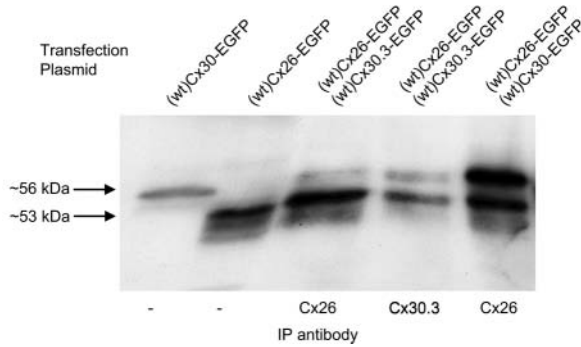
Fig. 8. Immunoprecipitation analysis. Cells were transfected with a Cx-EGFP construct (first two lanes) or pairs of Cx-EGFP constructs immunoprecipitated with either Cx26 or Cx30.3 antibodies. Western blotting was performed using an anti-EGFP-HRP antibody to detect any Cx-EGFP chimeric protein present. The Cx26 antibody immunoprecipitated Cx26-EGFP+Cx30-EGFP or Cx26-EGFP+Cx30.3-EGFP. In addition, the Cx30.3 antibody immunoprecipitated Cx26-EGFP+Cx30.3-EGFP. The size of the Cx26-EGFP band is ~53 kDa and both Cx30-EGFP and Cx30.3-EGFP were ~56 kDa. The interaction between Cx26 and Cx30 appears to be much stronger although this may be due to the higher levels of Cx26 and Cx30 expression compared to Cx30.3 seen in these experiments.

respect to the latter, (wt)Cx30.3 may need other co-factors to traffic to the plasma membrane of the keratinocyte, specifically those molecules that are present only in differentiated keratinocytes within the stratum granulosum.

The coexpression of wild-type connexins had an effect on the localisation of the two mutant connexins in particular (G11R)Cx30. These data suggest that the wild-type connexin protein may partially 'rescue' the trafficking defect inherent with the mutant protein. However, the aggregation of wild-type plus mutant connexons at the plasma membrane were small and punctuated, indicating that these 'rescued' channels were likely to be impaired or non-functional as large protein aggregates are required to facilitate intercellular communication (Bukauskas et al., 2000). In support of the latter, studies in HeLa cells have shown that overexpressing either (wt)Cx26 or (wt)Cx30 improved the trafficking of mutant Cx26 proteins but these channels had impaired dye permeability (Marziano et al., 2003; Thomas et al., 2004). The colocalisation analysis directly from the confocal images demonstrated the visual detection of protein aggregations at the plasma membrane and was suggestive of different combinations of direct connexin interactions.

The structure of a connexon resembles a hexameric barrel with six connexins occupying six vertices with the height of the barrel (the length of a connexon) estimated at about 7.5 nm making a gap junction channel 15 nm in length (Unger et al., 1999). The diameter of a connexon varies, and is 7 nm at the membrane region (Unger et al., 1999). Adjacent channels on a plaque are roughly 9 nm apart (Goodenough et al., 1996). These close proximities make the technique of FRET an ideal tool to investigate the formation and the interaction of connexons. FRET has been widely used to analyse molecular proximity and molecular interactions. It involves non-radioactive transfer of first-exited-state energy from an initially

excited molecule (referred as a donor) to another molecule (referred as the acceptor).

The differences in average FRET efficiency values between different homomeric wild-type connexins may be related to protein sequence homology and/or differences in their proximities, such as the size of connexons or the channel diameter at gap junctions (Table 2). They cannot, however, be used to interpret the arrangement of heteromeric/homomeric connexons. Their formations can be detected using the membrane cluster model (Dewey and Hammes, 1980), which relies on the FRET efficiency distributions against donor-acceptor concentration ratios (referred as D-A ratios) and acceptor concentrations (referred as A levels) to interpret the arrangement of interaction proteins. In general, if the arrangement of donor and acceptor molecules is completely clustered in a complex, FRET efficiencies are independent of A levels, but increase inversely with the D-A ratios. If donor and acceptor molecules are distributed randomly, FRET efficiencies increase with absolute A levels but are independent of the D-A ratios for a given total molecular density. For a mixture of clusters and randomly arranged molecules, FRET efficiencies increase with A levels, and increase inversely with the D-A ratios. So far, these models have been used to explain formations of molecular complexes in the plasma membrane and ER (Kenworthy et al., 2000; Silvius, 2003).

The membrane-clustering model was examined using the gap junction-like aggregates of cells that have previously been shown to have regular matrix structures (Unger et al., 1999). The membrane-clustering model gives the same interpretation using their FRET efficiency distributions. Taking the gap junction-like aggregates as positive controls, we found that FRET efficiencies within the cytoplasm of cells have identical distributions, an indication of clusters within the cytoplasm. As connexons are formed in the ER before being transported to the plasma membrane (Martin et al., 2001), these connexin clusters can only be connexons. Data in Fig. 7 show a decrease of FRET efficiency with D-A ratios, and a slight increase with A levels (except Cx30.3 and Cx30.3), a sign of the coexistence of energy transfers within the clusters as well as between clusters (random interaction). The energy transfer within connexon clusters demonstrates the existence of heteromeric connexons when donors and acceptors are tagged to different connexins, although such a sample is likely to have the mixture of both homomeric and heteromeric connexons.

Interestingly, in the coexpressed connexin combinations, we found ROIs with zero FRET efficiency in both the cytoplasm and at the plasma membrane, which were not seen in single wild-type connexin samples (Fig. 7). We speculate that both connexins dominantly formed their own homomeric connexons within this region. Although both homomeric connexons seem to be colocalized within microscopic resolution (>200 nm), they are in separate small groups, and the random energy transfer between them is too weak to detect.

In conclusion, these data indicate that there is evidence for multiple connexin interactions in keratinocytes (and, indeed in other cell types) with the formation of a number of different channel types. Thus, the effect of disease-associated Cx26 or Cx30 mutation may disrupt a number of different channel types to varying degrees of severity depending on the mutation.

References

Bevans, C. G., Kordel, M., Rhee, S. K. and Harris, A. L. (1998). Isoform composition of connexin channels determines selectivity among second messengers and uncharged molecules. *J. Biol. Chem.* **273**, 2808-2816.

Bukauskas, F. F., Jordan, K., Bukauskiene, A., Bennett, M. V., Lampe, P. D., Laird, D. W. and Verselis, V. K. (2000). Clustering of connexin 43-enhanced green fluorescent protein gap junction channels and functional coupling in living cells. *Proc. Natl Acad. Sci. USA* **97**, 2556-2561.

Cohen-Salmon, M., Ott, T., Michel, V., Hardelin, J. P., Perfettini, I., Eybalin, M., Wu, T., Marcus, D. C., Wangemann, P., Willecke, K. et al. (2002). Targeted ablation of connexin26 in the inner ear epithelial gap junction network causes hearing impairment and cell death. *Curr. Biol.* **12**, 1106-1111.

Common, J. E., Becker, D., Di, W. L., Leigh, I. M., O'Toole, E. A. and Kelsell, D. P. (2002). Functional studies of human skin disease- and deafness-associated connexin 30 mutations. *Biochem. Biophys. Res. Commun.* **298**, 651-656.

Common, J. E., Di, W. L., Davies, D., Galvin, H., Leigh, I. M., O'Toole, E. A. and Kelsell, D. P. (2003). Cellular mechanisms of mutant connexins in skin disease and hearing loss. *Cell Commun. Adhes.* **10**, 347-351.

Denoyelle, F., Weil, D., Maw, M. A., Wilcox, S. A., Lench, N. J., Allen-Powell, D. R., Osborn, A. H., Dahl, H. H., Middleton, A., Houseman, M. J. et al. (1997). Prelingual deafness: high prevalence of a 30delG mutation in the connexin 26 gene. *Hum. Mol. Genet.* **6**, 2173-2177.

Dewey, T. G. and Hammes, G. G. (1980). Calculation on fluorescence resonance energy transfer on surfaces. *Biophys. J.* **32**, 1023-1035.

Di, W. L., Common, J. E. and Kelsell, D. P. (2001a). Connexin 26 expression and mutation analysis in epidermal disease. *Cell Commun. Adhes.* **8**, 415-418.

Di, W. L., Rugg, E. L., Leigh, I. M. and Kelsell, D. P. (2001b). Multiple epidermal connexins are expressed in different keratinocyte subpopulations including connexin 31. *J. Invest. Dermatol.* **117**, 958-964.

Di, W. L., Monypenny, J., Common, J. E., Kennedy, C. T., Holland, K. A., Leigh, I. M., Rugg, E. L., Zicha, D. and Kelsell, D. P. (2002). Defective trafficking and cell death is characteristic of skin disease-associated connexin 31 mutations. *Hum. Mol. Genet.* **11**, 2005-2014.

Eidne, K. A., Kroeger, K. M. and Hanyaloglu, A. C. (2002). Applications of novel resonance energy transfer techniques to study dynamic hormone receptor interactions in living cells. *Trends Endocrinol. Metab.* **13**, 415-421.

Goldberg, G. S., Lampe, P. D. and Nicholson, B. J. (1999). Selective transfer of endogenous metabolites through gap junctions composed of different connexins. *Nat. Cell Biol.* **1**, 457-459.

Goldberg, G. S., Moreno, A. P. and Lampe, P. D. (2002). Gap junctions between cells expressing connexin 43 or 32 show inverse permselectivity to adenosine and ATP. *J. Biol. Chem.* **277**, 36725-36730.

Goodenough, D. A., Goliger, J. A. and Paul, D. L. (1996). Connexins, connexons, and intercellular communication. *Annu. Rev. Biochem.* **65**, 475-502.

Goodenough, D. A. and Paul, D. L. (2003). Beyond the gap: functions of unpaired connexon channels. *Nat. Rev. Mol. Cell Biol.* **4**, 285-294.

Gu, Y., Di, W. L., Kelsell, D. P. and Zicha, D. (2004). Quantitative fluorescence resonance energy transfer (FRET) measurement with acceptor photobleaching and spectral unmixing. *J. Microsc.* **215**, 162-173.

He, D. S., Jiang, J. X., Taffet, S. M. and Burt, J. M. (1999). Formation of heteromeric gap junction channels by connexins 40 and 43 in vascular smooth muscle cells. *Proc. Natl Acad. Sci. USA* **96**, 6495-6500.

Kelsell, D. P., Dunlop, J., Stevens, H. P., Lench, N. J., Liang, J. N., Parry, G., Mueller, R. F. and Leigh, I. M. (1997). Connexin 26 mutations in hereditary non-syndromic sensorineural deafness. *Nature* **387**, 80-83.

Kelsell, D. P., Di, W. L. and Houseman, M. J. (2001a). Connexin Mutations in Skin Disease and Hearing Loss. *Am. J. Hum. Genet.* **68**, 559-568.

Kelsell, D. P., Dunlop, J. and Hodgins, M. B. (2001b). Human diseases: clues to cracking the connexin code? *Trends Cell Biol.* **11**, 2-6.

Kenworthy, A. K., Petranova, N. and Edidin, M. (2000). High-resolution FRET microscopy of cholera toxin B-subunit and GPI-anchored proteins in cell plasma membranes. *Mol. Biol. Cell* **11**, 1645-1655.

Kudo, T., Kure, S., Ikeda, K., Xia, A. P., Katori, Y., Suzuki, M., Kojima, K., Ichinohe, A., Suzuki, Y., Aoki, Y. et al. (2003). Transgenic expression of a dominant-negative connexin26 causes degeneration of the organ of Corti and non-syndromic deafness. *Hum. Mol. Genet.* **12**, 995-1004.

Kumar, N. M. and Gilula, N. B. (1996). The gap junction communication channel. *Cell* **84**, 381-388.

Lal, R. and Lin, H. (2001). Imaging molecular structure and physiological function of gap junctions and hemijunctions by multimodal atomic force microscopy. *Microsc. Res. Tech.* **52**, 273-288.

Lauf, U., Giepmans, B. N., Lopez, P., Braconnot, S., Chen, S. C. and Falk, M. M. (2002). Dynamic trafficking and delivery of connexons to the plasma membrane and accretion to gap junctions in living cells. *Proc. Natl Acad. Sci. USA* **99**, 10446-10451.

Lippincott-Schwartz, J., Snapp, E. and Kenworthy, A. (2001). Studying protein dynamics in living cells. *Nat. Rev. Mol. Cell Biol.* **2**, 444-456.

Lucke, T., Choudhry, R., Thom, R., Selmer, I. S., Burden, A. D. and Hodgins, M. B. (1999). Upregulation of connexin 26 is a feature of keratinocyte differentiation in hyperproliferative epidermis, vaginal epithelium, and buccal epithelium. *J. Invest. Dermatol.* **112**, 354-361.

Martin, P. E., Blundell, G., Ahmad, S., Errington, R. J. and Evans, W. H. (2001). Multiple pathways in the trafficking and assembly of connexin 26, 32 and 43 into gap junction intercellular communication channels. *J. Cell Sci.* **114**, 3845-3855.

Marziano, N. K., Casalotti, S. O., Portelli, A. E., Becker, D. L. and Forge, A. (2003). Mutations in the gene for connexin 26 (GJB2) that cause hearing loss have a dominant negative effect on connexin 30. *Hum. Mol. Genet.* **12**, 805-812.

Meyer, C. G., Amedofu, G. K., Brandner, J. M., Pohland, D., Timmann, C. and Horstmann, R. D. (2002). Selection for deafness? *Nat. Med.* **8**, 1332-1333.

Morley, S. M., Dundas, S., James, J., Brown, R. A., Sexton, C., Navsaria, H. A., Leigh, I. M. and Lane, E. B. (1995). Temperature sensitivity of the keratin cytoskeleton and delayed spreading of keratinocyte lines derived from EBS patients. *J. Cell Sci.* **108**, 3463-3471.

Plantard, L., Huber, M., Macari, F., Meda, P. and Hohl, D. (2003). Molecular interaction of connexin 30.3 and connexin 31 suggests a dominant-negative mechanism associated with erythrokeratodermia variabilis. *Hum. Mol. Genet.* **12**, 3287-3294.

Richard, G. (2003). Connexin gene pathology. *Clin. Exp. Dermatol.* **28**, 397-409.

Richard, G., Rouan, F., Willoughby, C. E., Brown, N., Chung, P., Ryynanen, M., Jabs, E. W., Bale, S. J., DiGiovanna, J. J., Uitto, J. et al. (2002). Missense Mutations in GJB2 Encoding Connexin-26 Cause the Ectodermal Dysplasia Keratitis-Ichthyosis-Deafness Syndrome. *Am. J. Hum. Genet.* **70**, 1341-1348.

Saez, J. C., Contreras, J. E., Bukauskas, F. F., Retamal, M. A. and Bennett, M. V. (2003). Gap junction hemichannels in astrocytes of the CNS. *Acta Physiol. Scand.* **179**, 9-22.

Sekar, R. B. and Periasamy, A. (2003). Fluorescence resonance energy transfer (FRET) microscopy imaging of live cell protein localizations. *J. Cell Biol.* **160**, 629-633.

Silvius, J. R. (2003). Fluorescence energy transfer reveals microdomain formation at physiological temperatures in lipid mixtures modeling the outer leaflet of the plasma membrane. *Biophys. J.* **85**, 1034-1045.

Teubner, B., Michel, V., Pesch, J., Lautermann, J., Cohen-Salmon, M., Sohl, G., Jahnke, K., Winterhager, E., Herberhold, C., Hardelin, J. P. et al. (2003). Connexin30 (Gjb6)-deficiency causes severe hearing impairment and lack of endocochlear potential. *Hum. Mol. Genet.* **12**, 13-21.

Thomas, T., Telford, D. and Laird, D. W. (2004). Functional domain mapping and selective trans-dominant effects exhibited by Cx26 disease-causing mutations. *J. Biol. Chem.* **279**, 19157-19168.

Unger, V. M., Kumar, N. M., Gilula, N. B. and Yeager, M. (1999). Three-dimensional structure of a recombinant gap junction membrane channel. *Science* **283**, 1176-1180.

White, T. W. and Paul, D. L. (1999). Genetic diseases and gene knockouts reveal diverse connexin functions. *Annu. Rev. Physiol.* **61**, 283-310.

Willecke, K., Eiberger, J., Degen, J., Eckardt, D., Romualdi, A., Guldenagel, M., Deutsch, U. and Sohl, G. (2002). Structural and functional diversity of connexin genes in the mouse and human genome. *Biol. Chem.* **383**, 725-737.

Wouters, F. S., Bastiaens, P. I., Wirtz, K. W. and Jovin, T. M. (1998). FRET microscopy demonstrates molecular association of non-specific lipid transfer protein (nsL-TP) with fatty acid oxidation enzymes in peroxisomes. *EMBO J.* **17**, 7179-7189.

Yeager, M., Unger, V. M. and Falk, M. M. (1998). Synthesis, assembly and structure of gap junction intercellular channels. *Curr. Opin. Struct. Biol.* **8**, 517-524.

Zelante, L., Gasparini, P., Estivill, X., Melchionda, S., D'Agruma, L., Govea, N., Mila, M., Monica, M. D., Lutfi, J., Shohat, M. et al. (1997). Connexin26 mutations associated with the most common form of non-syndromic neurosensory autosomal recessive deafness (DFNB1) in Mediterraneans. *Hum. Mol. Genet.* **6**, 1605-1609.